Structures of the *Toxoplasma* gliding motility adhesin

Gaojie Song[a,b] and Timothy A. Springer[a,b,1]

[a]Program in Cellular and Molecular Medicine and Division of Hematology, Department of Medicine, Boston Children's Hospital, Boston, MA 02115; and [b]Department of Biological Chemistry and Molecular Pharmacology, Harvard Medical School, Boston, MA 02115

Contributed by Timothy A. Springer, February 18, 2014 (sent for review January 16, 2014; reviewed by K. Christopher Garcia and L. David Sibley)

Micronemal protein 2 (MIC2) is the key adhesin that supports gliding motility and host cell invasion by *Toxoplasma gondii*. With a von Willebrand factor A (VWA) domain and six thrombospondin repeat domains (TSR1–6) in its ectodomain, MIC2 connects to the parasite actomyosin system through its cytoplasmic tail. MIC2-associated protein (M2AP) binds noncovalently to the MIC2 ectodomain. MIC2 and M2AP are stored in micronemes as proforms. We find that the MIC2–M2AP ectodomain complex is a highly elongated 1:1 monomer with M2AP bound to the TSR6 domain. Crystal structures of N-terminal fragments containing the VWA and TSR1 domains for proMIC2 and MIC2 reveal a closed conformation of the VWA domain and how it associates with the TSR1 domain. A long, proline-rich, disulfide-bonded pigtail loop in TSR1 overlaps the VWA domain. Mannose α-C-linked to Trp-276 in TSR1 has an unusual $^1C_4$ chair conformation. The MIC2 VWA domain includes a mobile α5-helix and a 22-residue disordered region containing two disulfide bonds in place of an α6-helix. A hydrophobic residue in the prodomain binds to a pocket adjacent to the α7-helix that pistons in opening of the VWA domain to a putative high-affinity state.

Toxoplasmosis, caused by *Toxoplasma gondii*, can be fatal in immune-compromised individuals. Like *Plasmodium*, *Toxoplasma* is a member of the phylum *Apicomplexa*. Apicomplexans have a type of motility unknown in other phyla, gliding motility. Proteins required for gliding are secreted at the apical end from micronemes. Orthologs for the primary adhesin are known as micronemal protein 2 (MIC2) in *Toxoplasma* and thrombospondin repeat anonymous protein (TRAP) in *Plasmodium*. Like TRAP (1), MIC2 is required both for gliding motility and host cell invasion (2, 3). The ectodomain binds to extracellular ligands, and the cytoplasmic domain connects to the motility apparatus (4). During invasion, MIC2 moves from the apical to the posterior end as the parasite penetrates the host cell, and is finally shed before parasitophorous vacuole closure (5). MIC2-associated protein (M2AP) is required for MIC2 transport through the secretory network (2, 6, 7).

Previous structures of *Plasmodium falciparum* and *Plasmodium vivax* TRAP revealed the VWA domain in both open and closed conformations (8). The TSR domain was disordered when associated with the closed VWA conformation. However, the open VWA conformation revealed that disulfide-linked segments N- and C-terminal to the VWA domain underwent large conformational change to a β-ribbon structure. In turn, this extensible β-ribbon overlapped with the TSR domain to create a rigid unit.

MIC2 has six TSR domains compared with one in TRAP (Fig. 1*A*). Most notably, all orthologs but *Plasmodium* TRAP contain a 14- to 17-residue proline-rich insertion in the TSR1 domain β2–β3 loop (Fig. 1 *A* and *C*); this insertion is lacking in MIC2 TSR2-6 (Fig. 1*D*). The sequence of extensible β-ribbon segments A and B is highly conserved among species in *Plasmodium* but diverges in other genera (Fig. 1*C*) (8). Moreover, *Toxoplasma* and *Neospora* MIC2 but not other orthologs contain a propeptide (Fig. 1*A*). Finally, MIC2 has been reported to be a trimeric complex with M2AP (9), whereas TRAP is a monomer. Here, we address these issues structurally. We report the shape and domain arrangement of the MIC2–M2AP complex. Crystal structures of the pro and mature forms of the VWA–TSR1 tandem reveal surprising differences from TRAP, including a pigtail that projects from the TSR domain and associates with ribbon B and the VWA domain.

Results

We tested secretion from HEK293T transfectants of MIC2 fragments truncated after each TSR domain (Fig. 1 *D* and *E*). Pro and mature forms ending after TSR1 (residues 30–337 and 67–337, respectively) were each well expressed (Fig. 1*E*, lanes 1 and 2). Truncations after TSR domains 2–5 were also well expressed (Fig. 1*E*, lanes 3–6). However, truncation in the homologous position at residue 645 after TSR6 (Fig. 1*D*) yielded greatly reduced secretion (Fig. 1*E*, lane 7). C-terminal extension to residue 651 and 660 successively improved expression (Fig. 1*E*, lanes 8 and 9). Thus, despite its mucin-like (Pro, Gly, Ser, and Thr-rich) sequence (Fig. 1*D*), this segment is important for folding and/or secretion.

The MIC2 ectodomain and its complex with M2AP eluted earlier in gel filtration than expected for monomeric, globular proteins (9) (Fig. 2*A*). To determine whether this finding resulted from multimerization or a highly elongated structure, we used multiangle light scattering, which determines absolute molecular mass (Fig. 2*B*). The molecular mass of the complex was 107,600 Da, close to the calculated mass of 108,700 Da for a 1:1 MIC2–M2AP complex. Thus, MIC2–M2AP is a highly elongated monomer.

MIC2 truncations (Fig. 1 *D* and *E*) were used to localize M2AP binding. M2AP binds to two different MIC2 constructs ending with TSR6, 67–679 (Fig. 2*A*) and 67–660 (Fig. 2*C*). In contrast, MIC2 constructs ending with TSR5 (Fig. 2*D*), TSR4, or TSR1 did not bind M2AP.

Envelopes in solution of the MIC2–M2AP complex and MIC2 ATSR1 and ATSR4 fragments were determined by small angle X-ray scattering (SAXS) (Fig. 2 *E* and *F*). Comparisons of the solution envelopes of the three constructs (Fig. 2*G*) allows us to orient them as shown in Fig. 2*G* with the VWA domain to the left and to schematize their domain architecture as shown in Fig. 2*H*. The SAXS results confirm that MIC2 is a highly elongated

Significance

Structures of the major adhesin in *Toxoplasma* show how its ligand-binding domain is displayed above the cell surface at the tip of a stalk with six elongated domains. A prodomain inhibits conformational change from closed to open. An associating protein binds to the most membrane-proximal domain. Comparison with orthologues in *Plasmodium* reveals remarkable specializations as well as similarities between diverse apicomplexans.

Author contributions: T.A.S. designed research G.S. performed research; G.S. and T.A.S. analyzed data; and G.S. and T.A.S. wrote the paper.

Reviewers: K.C.G., Stanford University; L.D.S., Washington University School of Medicine.

The authors declare no conflict of interest.

Data deposition: The atomic coordinates have been deposited in the Protein Data Bank, www.pdb.org (PDB ID codes 4OKR and 4OKU).

[1]To whom correspondence should be addressed. E-mail: timothy.springer@childrens.harvard.edu.

This article contains supporting information online at www.pnas.org/lookup/suppl/doi:10.1073/pnas.1403059111/-/DCSupplemental.

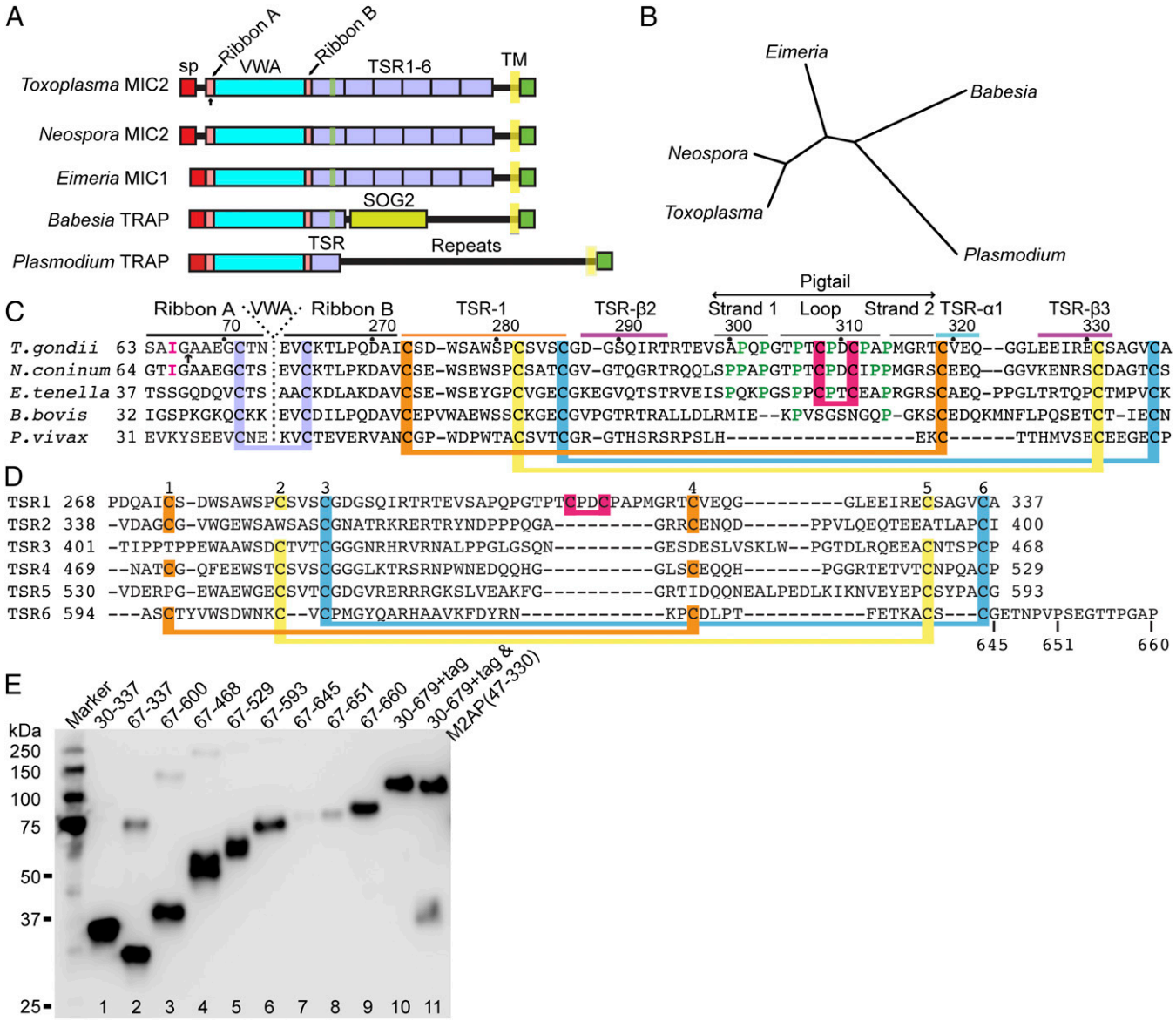

Fig. 1. MIC2 and its orthologs. (*A*) Currently known MIC2 orthologs. (*B*) Phylogenetic tree based on alignment of ribbon A through TSR1 sequence in *A*. (*C*) Alignment of ribbon and TSR1 sequences. Disulfide-bonded cysteines are connected. Prolines in pigtail are green. Dots mark decadal residues. An arrow marks cleavage of the propeptide and its key Ile is pink. (*D*) *T. gondii* MIC2 TSR domains. Putative disulfide linkages in TSR2-6 are assigned by homology to TSR1. (*E*) Construct expression assessed by anti-His Western blotting with equal quantities of transient HEK293T transfection supernatants subjected to reducing SDS 12.5% PAGE.

monomer and that M2AP binds to TSR6. Together the six TSR domains form a rod with limited flexibility and a bend near the middle. The long axis of M2AP appears perpendicular to the rod. The complex appears overall as a long leg, slightly flexed at the knee, with M2AP forming the foot.

Crystal structures were determined for VWA–TSR1 fragments of MIC2 (residues 67–337) and proMIC2 (residues 30–337) at 2.6 and 3.2 Å, respectively (Table S1). Each has two molecules per asymmetric unit with nearly identical VWA/TSR1 domain orientations. The structures show the VWA domain in a closed conformation, the TSR1 domain, and a long pigtail extending from TSR1 that contacts the VWA domain (Fig. 3*A*).

The positions of the MIC2 VWA domain β6–α7 loop and α7-helix are similar to those in closed conformations of TRAP and integrin αI domains (Fig. 3 *A*–*C*). Integrin αI domains bind ligand to their metal ion-dependent adhesion sites (MIDAS), which include three loops and a Mg^{2+} ion (Fig. 3*D*). The MIC2 MIDAS appears to have lost Mg^{2+} and deformed from the closed conformation as a consequence of crystallization at low pH of 4.6 and 3.7. The pK of Asp is 3.9, and because of Coulomb's law and the close proximity of Asp-82 and Asp-188 (Fig. 3*E*), it is likely that at least one of these residues is protonated. Ser-86 at the tip of the β1–α1 loop moves inward compared with closed integrin αI domains, so that its side chain oxygen takes the place normally occupied by Mg^{2+} (Fig. 3 *D* and *E*). Side chain hydrogen bonds of Ser-86 to Ser-84 and Asp-188 in MIC2 (Fig. 3*E*) replace metal ion coordinations to Ser-139 and Asp-239 in closed integrin αI domains (Fig. 3*D*).

MIC2 has 22 disordered residues instead of the α6-helix and α6–β6 loop found in TRAP and other VWA domains (Figs. 3 *A* and *B* and 4 *A*–*C*). The α6-helix in TRAP is stabilized by its Phe-198 residue, which packs in a hydrophobic pocket between the α5-helix and the protein core (Fig. 4*C*). In *Toxoplasma*, *Babesia*, *Neospora*, and *Eimeria*, the corresponding residue is a Glu,

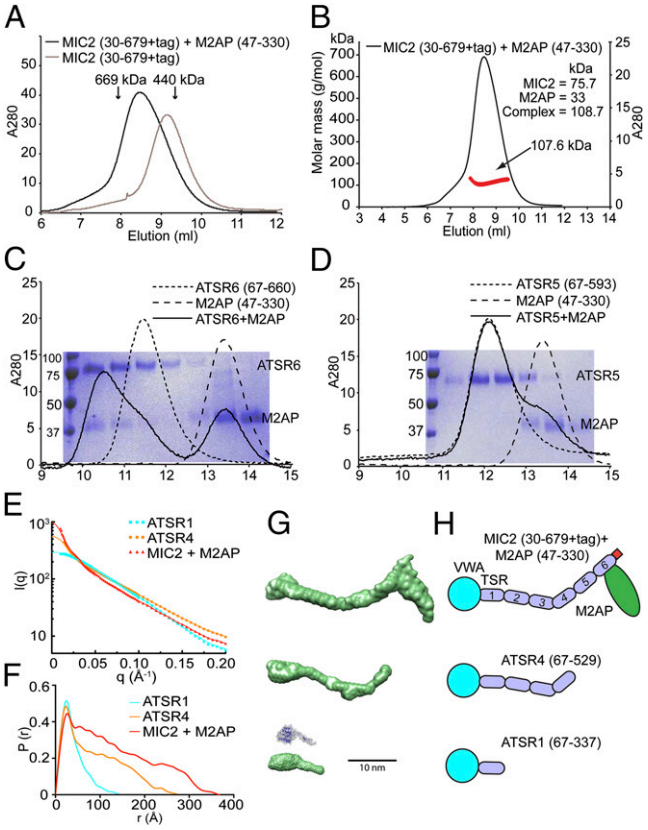

Fig. 2. Architecture of MIC2–M2AP. (*A*) Superdex S200 of MIC2–M2AP complex and MIC2 alone. (*B*) Absolute mass of MIC2–M2AP measured by multiangle light scattering. (*C* and *D*) ATSR6, but not ATSR5, forms a complex with M2AP, as detected by gel filtration and SDS/PAGE (*Inset*) of corresponding complex fractions. (*E*) Raw SAXS data (points) and fits (lines). (*F*) Distance distribution functions. (*G*) SAXS envelopes (green surfaces). The MIC2 crystal structure is shown above the ATSR1 SAXS envelope. (*H*) Schematic diagrams of domain architecture.

destabilizing both the α6- and α5-helices. Remarkably, four apparently disulfide-bonded cysteines are located in or adjacent to the disordered region (Fig. 4*D*). A highly entropic SGTSDDDS sequence (Fig. 4*D*) may contribute to disorder. In TRAP, the corresponding α6–β6 loop contains a single disulfide and juts out from the body of the domain (Fig. 4*C*).

Neighboring this disordered segment, the α5-helix in MIC2 shows different conformations in molecules A and B in the crystal lattice (Fig. 4 *A* and *B*). In one conformation, similar to that seen previously in a fragment of the MIC2 VWA domain (10), the α5-helix unwinds at its middle, and its N-terminal portion invades space occupied by the α6-helix in other VWA domains (Fig. 4*A*). The invading α5-helix conformation is stabilized by binding of Phe-195 to a pocket created by an unusually small side chain in the β4-strand at Gly-185 (Fig. 4*A*).

The proline-rich insert in TSR1 of MIC2 (Fig. 1*C*) forms a long pigtail that extends from the N-terminal end of the TSR domain (Figs. 3*A* and 5) and increases its length by about 50%. The pigtail interacts with the VWA domain and extensible ribbon B, burying a total of 1,395 Å^2 of solvent-accessible surface area. Compared with the closed conformation of TRAP, in which the TSR domain and C-terminal half of extensible ribbon B are disordered (Fig. 3*B*) (8), these regions in MIC2 are ordered by interaction of the pigtail with the VWA domain and ribbon B. The turn at the tip of the pigtail is stabilized both by the disulfide between Cys-308 and Cys-311 and a β-turn hydrogen bond between their backbones (Fig. 5*C*).

The orientation of the VWA and TSR domains differ by 9° and 5° between molecules A and B in MIC2 and proMIC2 crystal lattices, respectively. During flexion between VWA and TSR, the tip-proximal portion of the pigtail, residues 305–313, moves with its interacting VWA partner. In contrast, the TSR-proximal pigtail, residues 299–303 (strand 1) and 315–318 (strand 2), moves with the TSR domain and ribbon B residues 268–271. The two pigtail strands and ribbon B form a plait that extends into the TSR domain to form a rigid plait–TSR domain unit (Fig. 5*C*).

The plait is secured by networks of hydrogen bonds (Fig. 5*C*). Three backbone hydrogen bonds link ribbon B residues 269 and 271 to pigtail residues 302 and 317. Another backbone hydrogen bond links strand A residue Thr-72 to strand B residue Pro-268 (Fig. 5*C*). The strand A Thr-72 side chain hydrogen bonds to the local backbone and to the side chain of ribbon B residue Asp-270, which in turn hydrogen bonds to both the backbone and side chain of pigtail residue Arg-317 (Fig. 5*C*).

The closed structure of MIC2 suggests a facile mechanism for conversion to an open conformation. In TRAP, conversion of the closed to open VWA domain conformation is accompanied by C-terminal pistoning of the α7-helix and remodeling of ribbons A and B to form the extensible β-ribbon. In closed MIC2, although the tip-proximal pigtail interacts closely with the VWA domain, the interface is not markedly hydrophobic and is secured by only one side chain–backbone hydrogen bond. Importantly, most of the hydrogen bond network between the TSR-proximal pigtail strands and ribbons A and B can be preserved in an open conformation of MIC2, and hydrogen bonds between the two pigtail strands and the VWA domain are notably absent. Thus, although the extensible β-ribbon emerges de novo in the open conformation of TRAP (8), a portion of an analogous structure in MIC2 is preformed by the backbone hydrogen bonds described in the previous paragraph. We predict that, in the open conformation of MIC2, C-terminal pistoning of the α7-helix will be accompanied by conversion of the last one or two turns of α7-helix to extensible β-ribbon B as in TRAP, but ribbon B will form more hydrogen bonds to pigtail strands than to ribbon A. Additionally, the backbone hydrogen bond ladder may extend farther toward the pigtail tip during MIC2 opening. A nascent hydrogen bond network toward the pigtail tip is already exemplified. Backbone hydrogen bonds in molecule A link pigtail strand 1 residue 304 to pigtail strand 2 residue Pro-314 (Fig. 5*C*) and in molecule B link ribbon B residue 266 and pigtail strand 1 residue 305.

Aside from the pigtail loop, the structure of the MIC2 TSR1 domain is similar to that in TRAP (Fig. 5 *A* and *B*). TSR domains are stabilized by stacking of layers of residues on one face of the domain (11). The layers are marked with their one-letter codes in Fig. 5 *A* and *B*. The C-terminal end of the MIC2 TSR1 domain, including one disulfide, is disordered (Fig. 5*A*). In intact MIC2, the C-terminal disulfide-bonded loop and C terminus of each TSR domain may be ordered by interaction with and connection to the N-terminal portion of the following TSR domain (11). Such ordering is suggested by the rod-like structures of the tandem TSR modules in SAXS (Fig. 2*G*).

The electron density reveals that Trp-276 of MIC2 is mannosylated (Fig. 3 *A* and *F*). Trp-276 is followed by Trp-279 in the TSR layer (Fig. 1*C* and 5*A*), and thus is in a WXXW motif that often is mannosylated in TSR domains (12). NMR of a mannosylated peptide has shown that mannose is α-linked to the CD1 atom of the Trp indole ring and that the mannose predominantly adopts an unusual $^1C_4$-chair conformation (13). In the $^1C_4$-chair conformation, the substituents on the mannopyranosyl ring, including the glycosidically linked CD1 atom of Trp, are reversed from their axial and equatorial positions compared with the usual $^4C_1$-chair conformation (13). We could unequivocally assign the $^1C_4$-chair α-mannosyl conformation, because the equatorial glycosidic bond projects the mannose ring parallel to

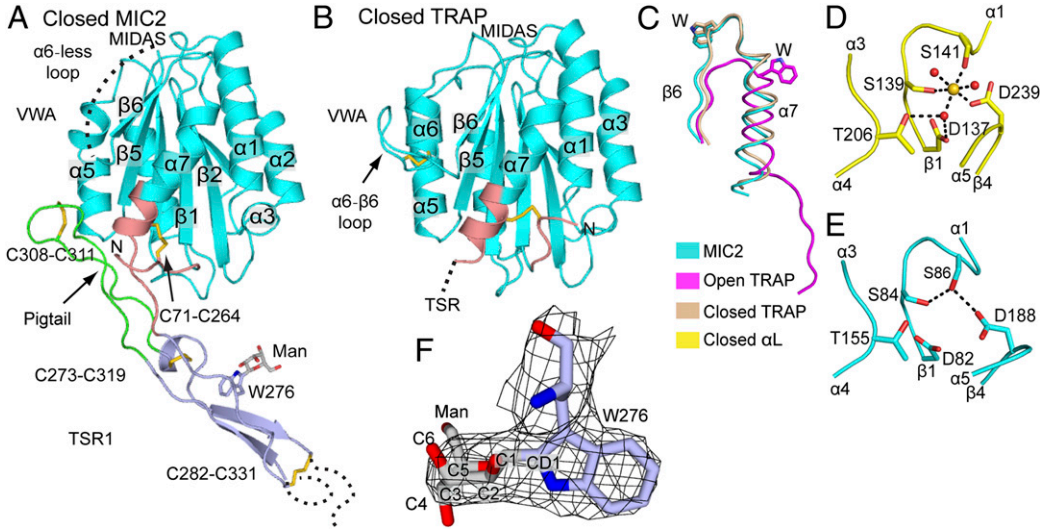

Fig. 3. Crystal structure of MIC2. (*A* and *B*) Ribbon diagrams of *Toxoplasma* MIC2 VWA–TSR1 fragment (*A*) and TRAP in closed conformation (*B*). VWA, ribbons A and B, pigtail, and TSR1 are colored cyan, magenta, green and light blue, respectively. Disulfide bonds (yellow), Trp276, and mannose are shown in stick. Dashes indicate disordered regions. (*C*) Comparisons of VWA β6-α7 regions in closed and open conformations. Fragments are in identical orientations after superposition on the VWA domain. Homologous Trp side chains are shown in stick. (*D* and *E*) MIDAS loops of closed integrin α_L αI domain (PDB ID 1MJN, *D*) and MIC2 (*E*). (*F*) $2F_o - F_c$ 1σ density (mesh) for α-mannosyl Trp276.

the long axis of the Trp side chain. In contrast, the α-mannose ring would project perpendicular to this axis in the $^4C_1$-chair conformation. Comparison with structures cited by Buettner et al. (12) suggests that $^1C_4$-chair C-α-mannosyl Trp has not previously been built in a crystal structure.

ProMIC2 differs from MIC2 structures only in the portion of the prodomain for which density is present, residues 62–66, and in the conformation of the following residues up to the disulfide linkage between ribbons A and B (Fig. 6 *A* and *B*). Notably, the side chain of propeptide residue Ile-65 binds in a hydrophobic cavity between the α1- and α7-helices (Fig. 6*B*). In the absence of the propeptide, a water molecule takes the place of Ile-65 (Fig. 6*A*). In TRAP VWA domain opening (8), the α7-helix undergoes pistoning and tilting that brings it into the position of the propeptide (Fig. 6*C*). Specifically, in the open TRAP conformation, Ile-227, equivalent to MIC2 Leu-260 (Fig. 6 *A* and *B*), occupies the same pocket as propeptide residue Ile-65 (Fig. 6*C*). Thus, the propeptide is predicted to inhibit VWA domain opening.

Discussion

With TRAP (8) and MIC2, diverse representatives of the major adhesin for apicomplexan gliding motility (Fig. 1 *A* and *B*) are now structurally characterized. We found surprising differences in the VWA domains of TRAP and MIC2. In place of the α6-helix and a jutting disulfide-bonded loop in TRAP, MIC2 contains 22 disordered residues. Of four cysteines in this region, only Cys-241 at its C-terminal border was ordered with a suggestion of

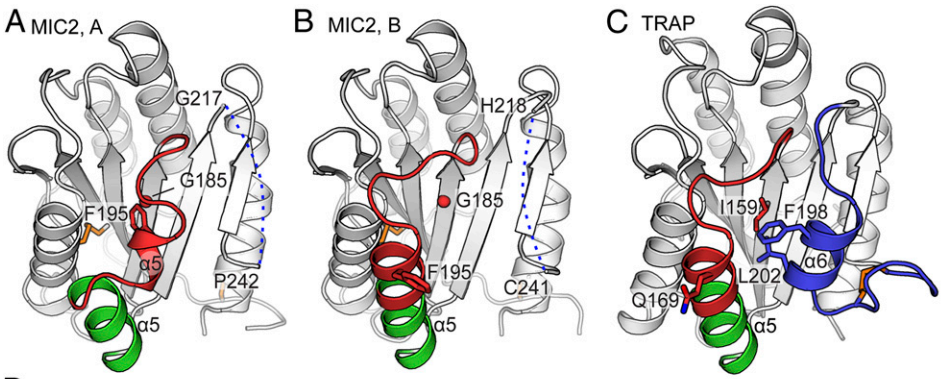

Fig. 4. Specializations of MIC2 VWA domain. (*A–C*) VWA domain conformations of MIC2 (*A*, chain A; *B*, chain B) and *P. falciparum* closed TRAP (*C*). Homologous regions are colored identically; the disordered region in MIC2 is blue in TRAP. (*D*) VWA domain sequence-structure alignment. Disordered residues are italicized. Dots mark decadal residues. The putative N-glycosylation site in the wild-type sequence is asterisked.

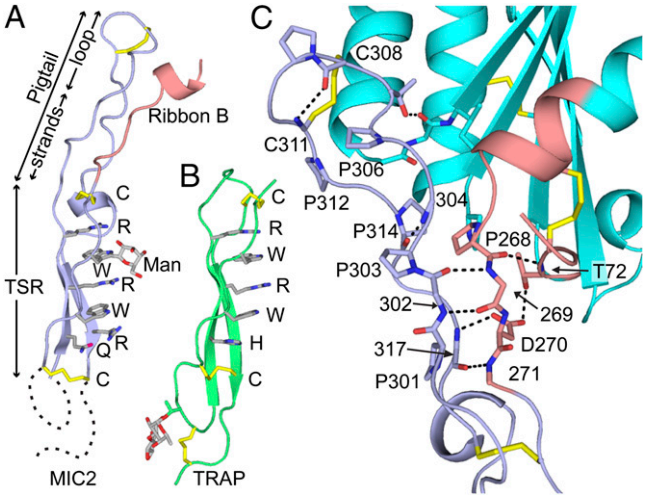

Fig. 5. The TSR domain, pigtail, and ribbon B. (*A* and *B*) The TSR domains of MIC2 (*A*) and TRAP (*B*) in identical orientations. Layer residues in TSR domains are shown as sticks and labeled. (*C*) Pigtail and VWA domain interactions. Key residues are shown as sticks and hydrogen bonds as dashes.

density for its disulfide. The N-terminal portion of the α5-helix showed alternative conformations in both MIC2 and proMIC2. The function of disorder and alternative conformations is unclear. To speculate, these regions might become ordered and assume different conformations when MIC2 binds different ligands.

MIDAS-containing VWA domains including integrin αI and βI domains (14), complement factor B (15), and TRAP (8) have been crystallized in both open and closed conformations. Open integrin I domains have ∼1,000-fold higher affinity than their closed counterparts (16–19). Increase in affinity comes from remodeling of two of the loops that surround the MIDAS, and an increase in strength of Mg^{2+} ion coordination to an acidic side chain in the ligand, which is coupled to changes in coordination of the Mg^{2+} ion to MIDAS loop residues. That the MIDAS is the ligand-binding site has been demonstrated structurally in both integrins and complement components (14, 15) and mutationally in TRAP (20). We crystallized MIC2 in the closed conformation. Although slightly deformed by low pH, the MIDAS in MIC2 is intact. By analogy to other MIDAS-containing VWA domains, we expect that MIC2 also has an open conformation with high affinity for ligand and will bind through its MIDAS Mg^{2+} ion and surrounding loops to ligand(s).

In the putative open conformation of MIC2, the TSR domain would piston along its long axis away from the VWA domain (8) as the VWA domain α7-helix unwinds at its C-terminal end to elongate and join ribbon B. As the pigtail loop slides down the side of the VWA domain during opening, we propose that hydrogen bonding between the two pigtail strands and ribbon B present in the closed conformation will extend further toward the tip of the pigtail loop and incorporate residues in ribbon B that unwind from the C-terminal end of the α7-helix. In TRAP, ribbons A and B form an antiparallel, extensible β-ribbon in the open conformation. In the open conformation of MIC2, pigtail strands 1 and 2 may largely replace ribbon A and form a three-stranded plait with ribbon B. This finding is consistent with divergence of ribbon A sequence from *Plasmodium* in other apicomplexans and its shortening by propeptide cleavage in *Toxoplasma* and *Neospora* (Fig. 1*C*).

Propeptide residue Ile-65 blocks α7-helix movement to the open conformation. Conversion of proMIC2 to MIC2 occurs after delivery from the microneme to the tachyzoite surface (21), thus priming MIC2 for opening. Intercellular adhesion molecule (ICAM)-1 may be one of the ligands of MIC2 (22). ICAM-1 is also a ligand of the integrin lymphocyte function-associated-1, which binds ICAM-1 to its αI domain MIDAS (14). However, the overall shapes of the loops around the MIDAS are quite different in MIC2 and the α_L αI domain. We were unable to find binding between ectodomains of MIC2 and ICAM-1 as assayed by a shift in elution in gel filtration, suggesting the K_D is above the concentrations used of 20 μM MIC2 and 4 μM ICAM-1.

Differing architectures of MIC2/TRAP orthologs (Fig. 1 *A* and *B*) correlate with differing parasitic habitats. The adhesin in coccidians (*Toxoplasma*, *Neospora*, and *Eimeria*) operates on tachyzoites in intestinal tracts; coccidians are transmitted through feces from one vertebrate to another. The adhesin in *Babesia* and *Plasmodium* operates on sporozoites that are transmitted from arthropod vector bites into the dermis of vertebrate hosts. The pigtail is highly conserved in *Coccidia* (Fig. 1*C*) and might act as a shield to protect the VWA–TSR domain interface from intestinal proteases. Adhesins neighbor major sheath components in coccidians (23) and *Plasmodium* (24) that share no structural resemblances. The much longer C-terminal, putatively unstructured sequences in *Babesia* and *Plasmodium*, compared with those in coccidian adhesins (Fig. 1*A*), may correlate with extension through thicker protein sheaths.

The M2AP binding site in MIC2 localizes to the TSR6 domain. Multiangle light scattering, gel filtration, and SAXS showed that in the MIC2 ectodomain complex with M2AP, the 6 TSR domains form a long leg that connects a VWA head to a foot-like projection formed by M2AP bound to TSR6. M2AP orthologs are found in all three coccidians (6) shown in Fig. 1, correlating with presence of six TSR domains in MIC2 (Fig. 1). M2AP might rest like a foot on the major tachyzoite sheath component, and help orient MIC2 so its VWA domain extends far above the tachyzoite surface for binding to ligands.

When the VWA domain binds ligand and the MIC2 cytoplasmic domain simultaneously engages the actin cytoskeleton, tensile force would be transmitted through the TSR domains. The force would energetically favor the more extended, open conformation of the VWA domain, and maintenance of adhesion despite force application. This model for regulation of stick-and-slip gliding motility has previously been discussed for TRAP (8).

Understanding of N- (25), O- (24), and C-glycosylation in apicomplexans is rapidly advancing. Asn in NX(S/T) sequons is N-glycosylated in *Toxoplasma* (25). MIC2 has 4 such sequons, and their deletion in the constructs used here was not deleterious for protein expression.

A CXX(S/T)CXXG motif in *Plasmodium* TSR domains is O-fucosylated when expressed in mammalian cells (8, 24). Although the homologous region in TSR1 of MIC2 was disordered (Fig. 5*A*), the fucosylation motif is present in TSR domain 1–5 of MIC2 (Fig. 1*C*) and the gene for the requisite glycosyl transferase, *POFUT2*, is present in *Toxoplasma*.

C-mannosylation of Trp in WXXW motifs occurs cotranslationally in the endoplasmic reticulum similarly to N-glycosylation

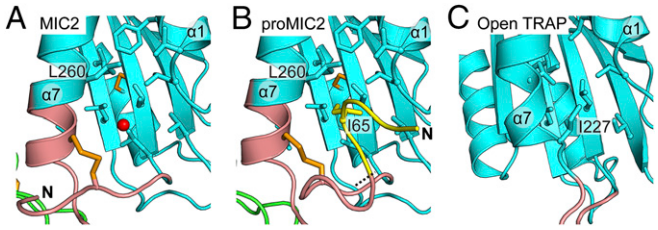

Fig. 6. The propeptide and its pocket. (*A–C*) Indicated structures are superimposed on the VWA domain. Coloring as in Fig. 3 *A–C*, with propeptide in yellow. Key residues are labeled and hydrophobic pocket residues are shown in stick. Dashes show the propeptide cleavage site. *N*-termini are labeled.

and is catalyzed by a homologous enzyme; the gene for a C-mannosyl transferase is present in *Toxoplasma* (12). C-α-mannosylation of Trp-276 in MIC2 expressed in mammalian cells suggests that this modification may also occur in *Toxoplasma* tachyzoites.

The significance of N-, O-, and C-linked carbohydrate modifications for development and infection by apicomplexans has yet to be tested. Whether to include such modifications is an important consideration in vaccine design. Glycans are substantial decorations of the protein surface that will alter epitopes wherever present.

Conditional knockout of MIC2 in *Toxoplasma* has shown that reduction of its expression severely compromises attachment and invasion and renders parasites avirulent in mice (3). Its essential role in infection makes MIC2 an attractive target for prophylactic and therapeutic vaccines in toxoplasmosis.

Methods

Protein Expression and Purification. *T. gondii* MIC2 and M2AP cDNA were generously provided by David Sibley (Division of Biology and Biomedical Sciences, Washington University in St. Louis, St. Louis) and Vern B. Carruthers (Department of Microbiology and Immunology, University of Michigan Medical School, Ann Arbor, MI). M2AP and fragments of MIC2 ending as shown in Fig. 1*D* were expressed in custom vectors (26) based on pLEXm (27) containing ligation-independent cloning sites, signal sequences and C-terminal His_6 tags. Mutations S158A, N357S, N463S, and N470D in MIC2 and N127R and S177N in M2AP removed N-glycosylation sites. HEK293T cells in DMEM with 10% (vol/vol) FBS at 70–80% confluence were transiently transfected with DNA:polyethylenimine at 1:1.5 wt/wt (28). Medium was changed to Freestyle 293 SFM (Invitrogen) 5 h later. Supernatants (1 L) were collected after 5–7 d, and adjusted to 20 mM Tris·HCL pH 7.5, 500 mM NaCl, 10 mM imidazole and 0.5 mM $NiCl_2$. Ni-NTA beads (5 mL) were added, then washed with 20 mM Tris pH 7.5, 500 mM NaCl, 20 mM imidazole and eluted with 20 mM Tris pH 7.5, 500 M NaCl, 300 mM imidazole. Concentrated proteins were subjected to Superdex S200 gel filtration in 20 mM Hepes 7.2, 200 mM NaCl, and 5 mM $MgCl_2$.

Multiangle Light Scattering. The miniDAWN triple angle detector (Wyatt Technology Corporation) at room temperature was used in line with a Superdex S200 column at 4 °C. Absolute mass was calculated using Wyatt's ASTRA software.

SAXS. SAXS measurements were at beam line X9 at the National Synchrotron Light Source (Upton, NY) with a high sensitivity 300K Pilatus detector at a distance of 3.4 m. Exposures (20 s) in triplicate were collected on protein at 2–4 mg/mL passed through a flow capillary. $I(0)$ and the pair distance distribution function $P(r)$ were calculated by circular averaging of the scattering intensities $I(q)$ and scaling using GNOM (29). Scattering from sample buffer of 20 mM Hepes pH 7.2, 200 mM NaCl, 5 mM $MgCl_2$ was subtracted. Guinier analysis showed no signs of radiation damage or aggregation. Twenty low-resolution ab initio models from GASBOR (30) were automatically averaged using DAMAVER (31). Models were converted to a surface map using SITUS (32).

Crystals. Protein concentrated to 5 mg/mL (MIC2) or 7 mg/mL (proMIC2) was stored at −80 °C. Crystallization was by hanging-drop vapor-diffusion. Crystals of MIC2 grew at 4 °C in 0.1 M sodium acetate pH 4.6, 0.2 M $(NH_4)_2SO_4$, 25% PEG 4000; crystals of proMIC2 grew at 20 °C in 0.2 M $(NH_4)_2SO_4$ and 20% PEG 3350 (measured pH of 3.9). Crystals were dipped in cryo-solution containing 20% (vol/vol) glycerol in mother liquor before flash-cooling in liquid nitrogen.

Structure Determination. Diffraction data collected at 100 K were processed with HKL2000 (33). Structure of MIC2 was solved by molecular replacement with PHENIX (34) using the truncated MIC2 VWA domain (PDB ID 2XGG) as search model. The proMIC2 structure was solved using our refined MIC2 structure. Models were built with COOT (35), refined with PHENIX including simulated annealing, and validated with MOLPROBITY (36).

ACKNOWLEDGMENTS. We thank beamlines X9A at National Synchotron Light Source and 24ID at Advanced Photon Source; Jianghai Zhu, Xianchi Dong, and Li-Zhi Mi for help with data collection and refinement; and Adem Koksal for help with SAXS data collection and processing. This work was supported by National Institutes of Health Grant AI095686.

1. Kappe SH, Buscaglia CA, Nussenzweig V (2004) Plasmodium sporozoite molecular cell biology. *Annu Rev Cell Dev Biol* 20:29–59.
2. Huynh MH, et al. (2003) Rapid invasion of host cells by Toxoplasma requires secretion of the MIC2-M2AP adhesive protein complex. *EMBO J* 22(9):2082–2090.
3. Huynh MH, Carruthers VB (2006) Toxoplasma MIC2 is a major determinant of invasion and virulence. *PLoS Pathog* 2(8):e84.
4. Jewett TJ, Sibley LD (2003) Aldolase forms a bridge between cell surface adhesins and the actin cytoskeleton in apicomplexan parasites. *Mol Cell* 11(4):885–894.
5. Carruthers VB, Giddings OK, Sibley LD (1999) Secretion of micronemal proteins is associated with toxoplasma invasion of host cells. *Cell Microbiol* 1(3):225–235.
6. Rabenau KE, et al. (2001) TgM2AP participates in Toxoplasma gondii invasion of host cells and is tightly associated with the adhesive protein TgMIC2. *Mol Microbiol* 41(3): 537–547.
7. Harper JM, et al. (2006) A cleavable propeptide influences Toxoplasma infection by facilitating the trafficking and secretion of the TgMIC2-M2AP invasion complex. *Mol Biol Cell* 17(10):4551–4563.
8. Song G, Koksal AC, Lu C, Springer TA (2012) Shape change in the receptor for gliding motility in Plasmodium sporozoites. *Proc Natl Acad Sci USA* 109(52):21420–21425.
9. Jewett TJ, Sibley LD (2004) The toxoplasma proteins MIC2 and M2AP form a hexameric complex necessary for intracellular survival. *J Biol Chem* 279(10):9362–9369.
10. Tonkin ML, Grujic O, Pearce M, Crawford J, Boulanger MJ (2010) Structure of the micronemal protein 2 A/I domain from Toxoplasma gondii. *Protein Sci* 19(10):1985–1990.
11. Tan K, et al. (2002) Crystal structure of the TSP-1 type 1 repeats: A novel layered fold and its biological implication. *J Cell Biol* 159(2):373–382.
12. Buettner FF, Ashikov A, Tiemann B, Lehle L, Bakker H (2013) C. elegans DPY-19 is a C-mannosyltransferase glycosylating thrombospondin repeats. *Mol Cell* 50(2): 295–302.
13. de Beer T, Vliegenthart JF, Löffler A, Hofsteenge J (1995) The hexopyranosyl residue that is C-glycosidically linked to the side chain of tryptophan-7 in human RNase Us is alpha-mannopyranose. *Biochemistry* 34(37):11785–11789.
14. Luo B-H, Carman CV, Springer TA (2007) Structural basis of integrin regulation and signaling. *Annu Rev Immunol* 25:619–647.
15. Forneris F, et al. (2010) Structures of C3b in complex with factors B and D give insight into complement convertase formation. *Science* 330(6012):1816–1820.
16. Shimaoka M, et al. (2003) Structures of the α L I domain and its complex with ICAM-1 reveal a shape-shifting pathway for integrin regulation. *Cell* 112(1):99–111.
17. Schürpf T, Springer TA (2011) Regulation of integrin affinity on cell surfaces. *EMBO J* 30(23):4712–4727.
18. Jin M, et al. (2006) Directed evolution to probe protein allostery and integrin I domains of 200,000-fold higher affinity. *Proc Natl Acad Sci USA* 103(15):5758–5763.
19. Zhu J, Zhu J, Springer TA (2013) Complete integrin headpiece opening in eight steps. *J Cell Biol* 201(7):1053–1068.
20. Matuschewski K, Nunes AC, Nussenzweig V, Ménard R (2002) Plasmodium sporozoite invasion into insect and mammalian cells is directed by the same dual binding system. *EMBO J* 21(7):1597–1606.
21. Carruthers VB, Sherman GD, Sibley LD (2000) The Toxoplasma adhesive protein MIC2 is proteolytically processed at multiple sites by two parasite-derived proteases. *J Biol Chem* 275(19):14346–14353.
22. Barragan A, Brossier F, Sibley LD (2005) Transepithelial migration of Toxoplasma gondii involves an interaction of intercellular adhesion molecule 1 (ICAM-1) with the parasite adhesin MIC2. *Cell Microbiol* 7(4):561–568.
23. He XL, Grigg ME, Boothroyd JC, Garcia KC (2002) Structure of the immunodominant surface antigen from the Toxoplasma gondii SRS superfamily. *Nat Struct Biol* 9(8): 606–611.
24. Doud MB, et al. (2012) Unexpected fold in the circumsporozoite protein target of malaria vaccines. *Proc Natl Acad Sci USA* 109(20):7817–7822.
25. Bushkin GG, et al. (2010) Suggestive evidence for Darwinian Selection against asparagine-linked glycans of Plasmodium falciparum and Toxoplasma gondii. *Eukaryot Cell* 9(2):228–241.
26. Zhou YF, et al. (2011) A pH-regulated dimeric bouquet in the structure of von Willebrand factor. *EMBO J* 30(19):4098–4111.
27. Aricescu AR, Lu W, Jones EY (2006) A time- and cost-efficient system for high-level protein production in mammalian cells. *Acta Crystallogr D Biol Crystallogr* 62(Pt 10):1243–1250.
28. Muller N, Girard P, Hacker DL, Jordan M, Wurm FM (2005) Orbital shaker technology for the cultivation of mammalian cells in suspension. *Biotechnol Bioeng* 89(4):400–406.
29. Svergun DI (1992) Determination of the regularization parameter in indirect-transform methods using perceptual criteria. *J Appl Cryst* 25:495–503.
30. Svergun DI, Petoukhov MV, Koch MH (2001) Determination of domain structure of proteins from X-ray solution scattering. *Biophys J* 80(6):2946–2953.
31. Volkov VV, Svergun DI (2003) Uniqueness of ab initio shape determination in small-angle scattering. *J Appl Cryst* 36:860–864.
32. Wriggers W (2010) Using Situs for the integration of multi-resolution structures. *Biophys Rev* 2(1):21–27.
33. Otwinowski Z, Minor W (1997) Processing of X-ray diffraction data collected in oscillation mode. *Methods Enzymol* 276:307–326.
34. Adams PD, et al. (2010) PHENIX: A comprehensive Python-based system for macromolecular structure solution. *Acta Crystallogr D Biol Crystallogr* 66(Pt 2):213–221.
35. Emsley P, Cowtan K (2004) Coot: Model-building tools for molecular graphics. *Acta Crystallogr D Biol Crystallogr* 60(Pt 12 Pt 1):2126–2132.
36. Davis IW, et al. (2007) MolProbity: All-atom contacts and structure validation for proteins and nucleic acids. *Nucleic Acids Res* 35(Web Server issue):W375–W383.